Biochemical and Biophysical Research Communications **287,** 468–473 (2001)
doi:10.1006/bbrc.2001.5617, available online at http://www.idealibrary.com on IDEAL®

An Investigation of Bisphosphonate Inhibition of a Vacuolar Proton-Pumping Pyrophosphatase

Christina M. Szabo and Eric Oldfield[1]

Department of Chemistry, University of Illinois at Urbana–Champaign, 600 South Mathews Avenue, Urbana, Illinois 61801

Received August 1, 2001

We report the results of a three-dimensional quantitative structure–activity relationship (3D-QSAR)/comparative molecular field analysis (CoMFA) of the activity of 18 bisphosphonates and imidodiphosphate in the inhibition of a mung bean (*Vigna radiata* L.) vacuolar proton pumping pyrophosphatase (V/H^+-PPase; EC 3.6.1.1). We find an experimental versus QSAR predicted pK_i^{app} R^2 value of 0.89, a cross-validated $R^2 = 0.77$, and a bootstrapped $R^2 = 0.89$ for 18 bisphosphonates plus imidodiphosphate over the 1.3 μM to 425 μM range of K_i^{app} values. We also demonstrate that this approach has predictive utility (a 0.26 pK_i^{app} rms error for three test sets of 3 activity predictions each), corresponding to about a factor of two error in K_i^{app} prediction. The 3D-QSAR/CoMFA approach provides a quantitative method for predicting the activity of V/H^+-PPase inhibitors and is likely to be of use in the design of novel pharmacological agents since all of the major human disease-causing parasitic protozoa contain large levels of pyrophosphate, together with V-type proton-pumping pyrophosphatases located in plant-like vacuoles (acidocalcisomes), which are absent in their mammalian hosts.

Key Words: **QSAR; CoMFA; pyrophosphatase; bisphosphonate.**

In recent work (1–4) using nuclear magnetic resonance spectroscopy we found evidence for the presence of high levels of pyrophosphate (diphosphate) in many of the major human disease-causing parasitic protozoa: *Trypanosoma cruzi* (1), *Trypanosoma brucei* (2), *Leishmania major* (2), *Toxoplasma gondii* (3, 4), *Plasmodium falciparum* (4) and *Cryptosporidium parvum* (4). These organisms are, respectively, the causative agents of Chagas' disease, human African sleeping sickness, visceral leishmaniasis, toxoplasmosis, malaria and cryptosporidiosis. These diseases afflict hundreds of millions of individuals in less developed nations as well as cause opportunistic infections in the immuno-compromised worldwide. The observation of large levels of PP_i led to the discovery (1, 2) of its primary localization in the acidocalcisome (5), an acidic vacuole present in each of the parasites. This then led to the discovery of plant-like (6) proton-pumping vacuolar pyrophosphatases in many disease-causing protozoa (7–10). In earlier work (11, 12), it was found that some pyrophosphate analogs, bisphosphonates (containing a non-hydrolysable P-C-P, rather than a P-O-P, backbone) as well as imidodiphosphate (containing a non-hydrolysable P-N-P group), were inhibitors of a plant (mung bean, *Vigna radiata* L.) V/H^+-PPase, and more recently Gordon-Weeks *et al.* reported a more extensive investigation of the structural aspects of the effectiveness of bisphosphonates as competitive inhibitors of the same enzyme (13). Several of these compounds have also been found to have inhibitory activity against the parasite enzymes (7–10). Given the potential importance of the V/H^+-PPase in parasite cell growth and since it is absent from human host cells, the plant results take on increased significance since they may help to facilitate the design of novel antiparasitic drugs. However, all of the reports to date discuss only *qualitative* structure–activity relationships. Here, we report the first *quantitative* structure–activity relationship (3D-QSAR) investigation, using a comparative molecular field analysis (CoMFA), of the inhibition of the *V. radiata* V/H^+-PPase by 18 bisphosphonates and by imidodiphosphate. In particular, we show that the activities of the V/H^+-PPase inhibitors can be predicted to within about a factor of two. In addition, the CoMFA results emphasize the overwhelming importance of electrostatic interactions between the bisphosphonates and the V/H^+-PPase.

MATERIALS AND METHODS

3D-QSAR/CoMFA. CoMFA was performed within the QSAR module of Cerius2 4.5 using default settings (14). Molecular mechan-

[1] To whom correspondence should be addressed. Fax: (217) 244-0997. E-mail: eo@chad.scs.uiuc.edu.

0006-291X/01 $35.00

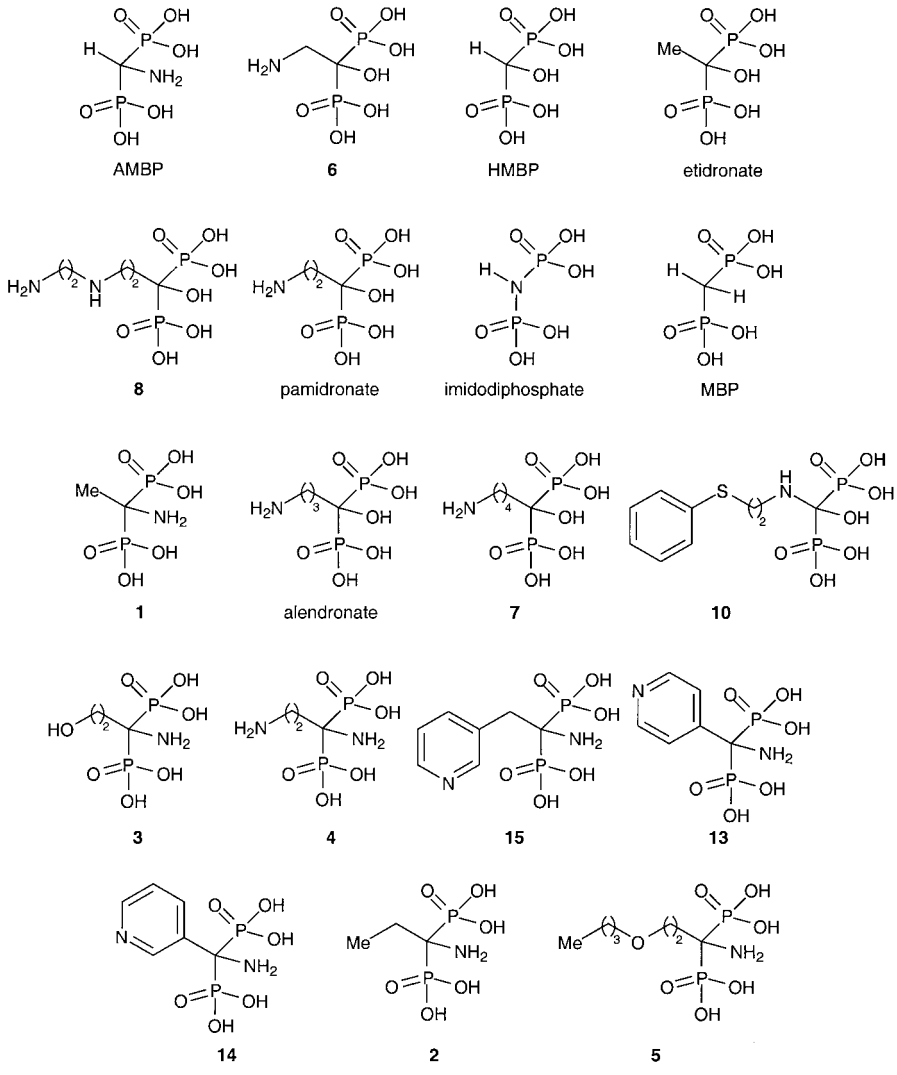

FIG. 1. Structures of the bisphosphonates investigated. The numbers and trivial names are those used in Refs. 12 and 13.

ics calculations for geometry optimization were performed by using a universal molecular mechanics force field (UFF), with a convergence criterion requiring a minimum energy change of 0.001 kcal/mol. Charge calculations were performed by using the Gasteiger method (15). The CoMFA calculated probe interaction energies on a rectangular grid around the surface of the aligned molecules. The atomic coordinates of the models were used to compute field values at each point on a 3D grid whose spacing was adjusted to 1.00 Å. CoMFA evaluated the energy between probes (H^+, CH_3, and hydrogen bond donor/acceptor) and a given inhibitor at a series of points defined by the rectangular grid. In a first set of calculations, we used 18 bisphosphonates plus imidodiphosphate to evaluate the QSAR of *V. radiata* V/H^+-PPase inhibitors. Then, to better estimate predictive ability we used three reduced training sets, each containing 16 compounds, to predict the activities of three test sets, each containing 3 compounds, as discussed in detail below.

RESULTS AND DISCUSSION

We show in Fig. 1 the structures of the 19 compounds investigated. The trivial names or the code numbers given by Gordon-Weeks *et al.* (13) are also shown in Fig. 1 and Table 1. The compounds are ordered in Fig. 1 in terms of increasing K_i^{app}. The corresponding K_i^{app} values for *V. radiata* V/H^+-PPase inhibition (in μM) for these compounds are given in Table 1 (12, 13). Bisphosphonate structures were generated for CoMFA investigation by using steepest descents followed by conjugate gradient, then Newton-Raphson, algorithms for geometry optimization, with no constraints on the internal geometry of the molecules, using the Minimizer function of the OFF Methods module in Cerius2 4.5 (14). Each molecule was aligned to the most active molecule (aminomethylene bisphosphonate, AMBP) acting as a template by performing an rms-fitting of the pharmacophoric atoms of each conformer to those of the template by using the shape reference alignment function of the QSAR module of Cerius2 4.5. The alignments of each structure, obtained through pairwise

TABLE 1

Experimental K_i^{app} and pK_i^{app} and Predicted pK_i^{app} Values for V/H^+-PPase Inhibitors and Statistical Results of 3D-QSAR/CoMFA Models

Compound	Experimental activity[a]		Predicted pK_i^{app}[b]			
	K_i^{app} (μM)	pK_i^{app}	Training set	3-compound test sets		
aminomethylene bisphosphonate (AMBP)	1.32 ± 0.05	5.88	5.69	5.64	5.72	5.73
6	1.92 ± 0.06	5.72	5.45	5.45	5.44	5.39
hydroxymethylene bisphosphonate (HMBP)	5.70	5.24	5.10	**5.07**	5.16	5.09
etidronate	6.5	5.19	5.10	5.07	**5.16**	5.09
8	6.58 ± 0.37	5.18	5.44	5.38	5.45	5.40
pamidronate	10.2 ± 0.51	4.99	4.49	4.56	4.49	**4.42**
imidodiphosphate	12	4.92	5.10	5.07	5.16	5.09
methylene bisphosphonate (MBP)	14.0 ± 0.811	4.85	5.10	5.07	**5.16**	5.09
1	18.7 ± 1.22	4.73	4.97	5.04	4.94	4.95
alendronate	33.7 ± 2.39	4.47	4.60	4.67	4.60	**4.54**
7	37.2 ± 1.84	4.43	4.34	4.42	4.34	4.27
10	62.0 ± 2.85	4.21	4.34	**4.42**	4.34	4.27
3	63.2 ± 1.22	4.20	3.73	3.83	3.73	3.67
4	173 ± 19.2	3.76	3.62	3.63	3.63	3.60
15	185 ± 12.9	3.73	3.62	3.63	3.63	**3.60**
13	227 ± 17.0	3.64	3.74	3.74	3.74	3.72
14	252 ± 17.4	3.60	3.62	3.63	**3.63**	3.60
2	313 ± 21.1	3.50	3.87	**3.98**	3.88	3.82
5	4.25 ± 31.4	3.37	3.73	3.83	3.73	3.67
R^{2}[c]			0.89	0.89	0.89	0.91
F_{test}[d]			27.9	23.1	22.1	28.2
R^{2}_{cv}[e]			0.77	0.72	0.78	0.79
R^{2}_{bs}[f]			0.89	0.90	0.89	0.91
N[g]			5	5	5	5
n[h]			19	16	16	16

[a] From Refs. 12 and 13.
[b] Bold values represent predicted activities of compounds that were not included in the training set.
[c] Correlation coefficient.
[d] Ratio of R^2 explained to unexplained = $R^2/(1–R^2)$.
[e] Cross-validated correlation coefficient after leave-one-out procedure.
[f] Average squared correlation coefficient calculated during the validation procedure.
[g] Optimal number of principal components.
[h] Number of observations.

superpositioning using the maximum common subgroup (MCSG) method, placed all 19 structures in the study table in the same reference frame as the shape reference compound. After visual inspection, the alignment was further refined by matching the P-C-P atoms of compound **10** and the P-N-P atoms of imidodiphosphate to the P-C-P atoms in AMBP (reference model) by an rms-fitting atom-matching algorithm in the Cerius2 4.5 software program. The aligned set of structures is shown in Fig. 2. For the aromatic species, the ring nitrogens were singly protonated while the aminoalkyl species had ammonium groups present. Monoprotonated phosphonate groups $[P(O)_2(OH)]^{-1}$ were used throughout. We then used CoMFA 3D-QSAR methodologies, as embodied in the Cerius2 4.5 suite of programs, to analyze the inhibition data shown in Table 1 using the relationship $pK_i^{app} = -\log_{10}(K_i^{app}, M)$. We performed a regression analysis of the inhibition results by using a genetic function approximation (GFA) algorithm (16) to obtain the following QSAR equation:

$$pK_i^{app} = 4.359 + 0.051 * \text{“}H^+/78\text{”} - 0.091 * \text{“}H^+/88\text{”} - 0.013 * \text{“}H^+/114\text{”} + 0.028 * \text{“}H^+/179\text{”} \quad [1]$$

where the descriptor, H^+, defines the corresponding probe interaction energy between a proton and the molecule of interest, at specified grid points. The locations of the descriptors in Eq. 1 are shown in Fig. 2. The optimal number of components in the final GFA model was determined by cross-validated R^2 and standard error prediction values, as obtained from the leave-one-out cross-validation technique. The GFA analysis gave a correlation coefficient of 0.89, with a cross-validated R^2_{cv} of 0.77, and an optimal number of components of 5. To obtain statistical confidence limits, the non-cross-

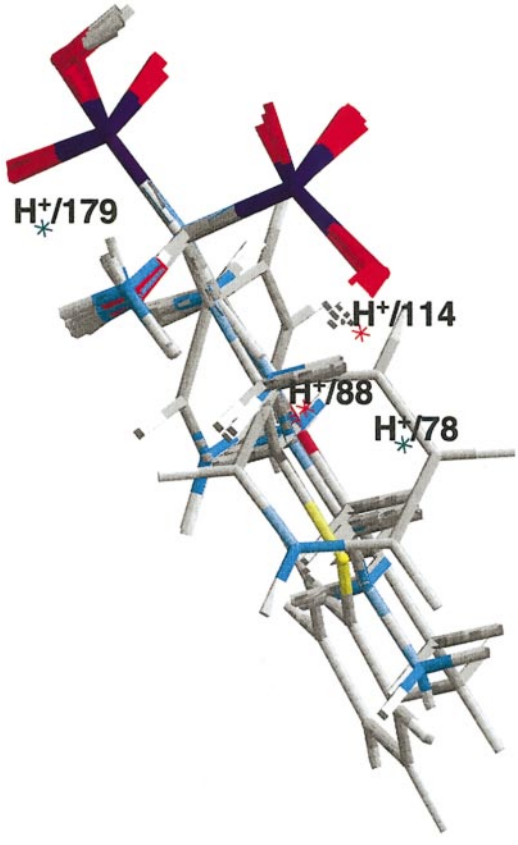

FIG. 2. Structure alignment: superposition of 19 compounds active in *V. radiata* L. V/H$^+$-PPase inhibition and descriptors from Eq. 1.

validated analysis was repeated with 10 bootstrap groups, which yielded an R^2_{bs} of 0.89. These statistical parameters are given in Table 1. Cross-validation provides information concerning the predictive ability of the QSAR data set by minimizing the occurrence of chance correlations in the QSAR model, and the bootstrapped R^2_{bs} value of 0.89 indicates a good degree of confidence in the analysis. Experimental and predicted pK_i^{app} values are shown in Table 1 and Fig. 3A. These results were of interest since they implied that it might be possible to predict K_i^{app} values for *V. radiata* V/H$^+$-PPase inhibition. The experimental range of activity (K_i^{app}) varies from 1.32 μM for AMBP to 425 μM for bisphosphonate **5**, as listed in Table 1. However, the R^2 values obtained from the results shown in Fig. 3A were lower than might typically be obtained for a larger training set and of course there may be additional uncertainties introduced by use of an intact tonoplast assay (as opposed to the use of a purified enzyme). Therefore, in order to better test the predictive ability of this 3D-QSAR/CoMFA model of V/H$^+$-PPase inhibition, we carried out three additional sets of calculations in which we deleted at random three (test set) points from the training set. The QSAR equations were then recomputed, the results of which were used to calculate the pK_i^{app} values for the three compounds in each test set (Table 1, bold).

The QSAR equations from the three reduced training sets were:

$$pK_i^{app} = 4.349 + 0.047 * \text{“H}^+/78\text{”} - 0.087 * \text{“H}^+/88\text{”} - 0.011 * \text{“H}^+/114\text{”} + 0.027 * \text{“H}^+/179\text{”} \quad [2]$$

$$pK_i^{app} = 4.308 + 0.054 * \text{“H}^+/78\text{”} - 0.102 * \text{“H}^+/88\text{”} - 0.011 * \text{“H}^+/113\text{”} + 0.035 * \text{“H}^+/179\text{”} \quad [3]$$

$$pK_i^{app} = 4.344 + 0.052 * \text{“H}^+/78\text{”} - 0.092 * \text{“H}^+/88\text{”} - 0.014 * \text{“H}^+/114\text{”} + 0.029 * \text{“H}^+/179\text{”} \quad [4]$$

The three sets of predicted pK_i^{app} values are shown in bold in Table 1, as are the R^2, R^2_{cv}, R^2_{bs} and F-test statistical results for each QSAR equation. Quite clearly, as can be seen from Eqs. 2–4, the new QSAR/CoMFA equations are extremely similar to the original model derived from the 19-compound training set. In addition, there is generally good agreement between the pK_i^{app} predictions for the nine test set compounds (Table 1, ◆ in Figs. 3B–3D) and the experimentally observed values with an rms error of 0.26, corresponding to an R^2 value of 0.80. The predictions of the activities of those compounds in the training sets are also shown (Table 1, ○ in Figs. 3B–3D). These results strongly suggest, therefore, that it is now possible to predict the pK_i^{app} values for V/H$^+$-PPase inhibition by these bisphosphonates and by imidodiphosphate to within about a factor of two (rmsd = 0.26). Based on the QSAR/CoMFA results (Eqs. 1–4), it is also apparent that the competitive inhibition of V/H$^+$-PPase by the bisphosphonates studied is overwhelmingly electrostatic in nature.

These QSAR results are to be compared with bisphosphonate inhibition of two other enzymes: farnesyl diphosphate synthase (FPPSase) and geranylgeranyl diphosphate synthase (GGPPase) (17–19). In the case of pamidronate and alendronate (Fig. 1), both molecules are ≈0.5 μM inhibitors of FPPSase. This is much lower than the ~10–30 μM values seen in V/H$^+$-PPase inhibition (Table 1), but in both enzymes the CoMFA results indicate that primarily electrostatic interactions dominate. In the case of FPPSase, it is thought that the potent nitrogen-containing bisphosphonates used in bone resorption therapy, which also have considerable activity against parasitic protozoa, act as carbocation transition state/reactive intermediate analogs (20). There are thus strong interactions

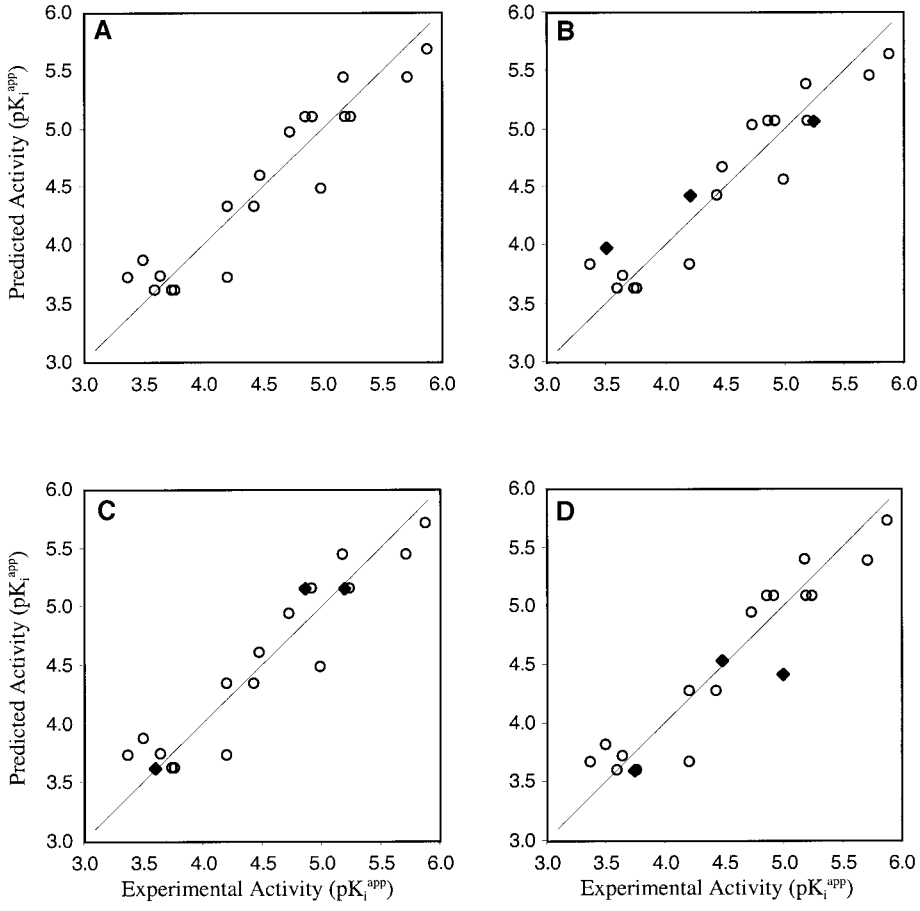

FIG. 3. Graph of CoMFA-derived QSAR predictions versus experimental bisphosphonate drug activity. (A) *V. radiata* V/H$^+$-PPase inhibition, 19-compound training set. (B–D) As A but 16-compound training set (○) and 3-compound test set (◆) predictions. The numerical and statistical results are given in Table 1. The line represents the ideal slope of 1.

between both the phosphonate headgroups and the ammonium (pyridinium) side-chains with FPPSase. With GGPPSase, however, hydrophobic interactions between the long alkyl/alkenyl sidechains of bisphosphonate inhibitors and the protein are very important (19) and the QSAR model is dominated by such steric/hydrophobic interactions. In the case of the V/H$^+$-PPase, however, hydrophobic interactions (manifest as contributions of CH_3 probe interaction energies to the calculated activity) are very small and indeed need not be incorporated into the QSAR model at all, as shown in Eqs. 1–4. Thus, bisphosphonates clearly inhibit different enzymes in quite different ways, through various types of interactions, ranging from overwhelmingly electrostatic with the V/H$^+$-PPase, to mixed electrostatic/H-bonding/steric with FPPSase, to primarily steric or hydrophobic with GPPSase (17–19).

In conclusion then, the results we have shown above are of importance for several reasons. First, they represent the first QSAR analysis of the inhibition of a vacuolar, proton-pumping pyrophosphatase by imidodiphosphate and by a series of bisphosphonates. Second, the results obtained indicate that it is possible to predict the activity (pK_i^{app}) of a broad range of V/H$^+$-PPase inhibitors with an rms error of 0.26, corresponding to an average K_i^{app} prediction error of about a factor of 2. Since all of the major human disease-producing protozoa possess this enzyme while their human hosts do not, V/H$^+$-PPase is a potentially attractive target for chemotherapeutic intervention and the results presented above indicate that it may now be possible to begin to use QSAR methods to develop improved inhibitors against both plant and parasite enzymes. Third, our QSAR results show the overwhelming dominance of purely electrostatic interactions in the bisphosphonate/imidodiphosphate V/H$^+$-PPase QSAR, unlike results recently obtained with these and related compounds acting as inhibitors of the prenyl synthases, FPPSase and GGPPSase (17–19), in which donor/acceptor and purely steric/hydrophobic/dispersive interactions become increasingly important, presumably due to the fact that the bisphosphonates mimic much larger carbocation species which are buried in the active sites of the FPP and GGPP synthases.

ACKNOWLEDGMENTS

This work was supported by the United States Public Health Service (NIH Grant GM-50694), by the American Heart Association, Midwest Affiliate (Grant 0151138Z), by the UNDP/World Bank/WHO Special Programme for Research and Training in Tropical Diseases (TDR) and by the National Computational Science Alliance (NSF grants MCB-000016N, MCB-000018N and MCB-000020N). C.M.S. was supported by NIH Training Grant GM-08276.

REFERENCES

1. Urbina, J. A., Moreno, B., Vierkotter, S., Oldfield, E., Payares, G., Sanoja, C., Bailey, B. N., Yan, W., Scott, D. A., Moreno, S., and Docampo, R. (1999) *Trypanosoma cruzi* contains major pyrophosphate stores, and its growth *in vitro* and *in vivo* is blocked by pyrophosphate analogues. *J. Biol. Chem.* **274,** 33609–33615.
2. Moreno, B., Urbina, J. A., Oldfield, E., Bailey, B. N., Rodrigues, C. O., and Docampo, R. (2000) ^{31}P NMR spectroscopy of *Trypanosoma brucei, Trypanosoma cruzi,* and *Leishmania major. J. Biol. Chem.* **275,** 28356–28362.
3. Rodrigues, C. O., Scott, D. A., Bailey, B. N., deSouza, W., Benchimol, M., Moreno, B., Urbina, J. A., Oldfield, E., and Moreno, S. N. J. (2000) Vacuolar proton pyrophosphatase activity and pyrophosphate (PPi) in *Toxoplasma gondii* as possible chemotherapeutic targets. *Biochem. J.* **349,** 737–745.
4. Moreno, B., Bailey, B. N., Luo, S., Martin, M. B., Kuhlenschmidt, M., Moreno, S. N. J., Docampo, R., and Oldfield, E. (2001) ^{31}P NMR of apicomplexans and the effects of risedronate on *Cryptosporidium parvum* growth. *Biochem. Biophys. Res. Commun.* **284,** 632–637.
5. Docampo, R., and Moreno, S. N. (2001) The acidocalcisome. *Mol. Biochem. Parasitol.* **114,** 151–159.
6. Drozdowicz, Y. M., and Rea, P. A. (2001) Vacuolar H(+) pyrophosphatases: from the evolutionary backwaters into the mainstream. *Trends Plant Sci.* **6,** 206–211.
7. Scott, D. A., de Souza, W., Benchimol, M., Zhong, L., Lu, H. G., Moreno, S. N., and Docampo, R. (1998) Presence of a plant-like proton-pumping pyrophosphatase in acidocalcisomes of *Trypanosoma cruzi. J. Biol. Chem.* **273,** 22151–22158.
8. Rodrigues, C. O., Scott, D. A., and Docampo, R. (1999) Characterization of a vacuolar pyrophosphatase in *Trypanosoma brucei* and its localization to acidocalcisomes. *Mol. Cell Biol.* **19,** 7712–7723.
9. Rodrigues, C. O., Scott, D. A., and Docampo, R. (1999) Presence of a vacuolar H^+-pyrophosphatase in promastigotes of *Leishmanai donovani* and its localization to a different compartment from the vacuolar H^+-ATPase. *Biochem. J.* **340,** 759–766.
10. McIntosh, M. T., Drozdowicz, Y. M., Laroiya, K., Rea, P. A., and Vaidya, A. B. (2001) Two classes of plant-like vacuolar-type H(+)-pyrophosphatases in malaria parasites. *Mol. Biochem. Parasitol.* **114,** 183–195.
11. Kim, E. J., Zhen, R. G., and Rea, P. A. (1994) Heterologous expression of plant vacuolar pyrophosphatase in yeast demonstrates sufficiency of the substrate-binding subunit for proton transport. *Proc. Natl. Acad. Sci. USA* **91,** 6128–6132.
12. Zhen, R. G., Baykov, A. A., Bakuleva, N. P., and Rea, P. A. (1994) Aminomethylene diphosphonate: A potent type-specific inhibitor of both plant and phototropic bacterial H^+-pyrophosphatases. *Plant Physiol.* **104,** 153–159.
13. Gordon-Weeks, R., Parmar, S., Davies, T. G., and Leigh, R. A. (1999) Structural aspects of the effectiveness of bisphosphonates as competitive inhibitors of the plant vacuolar proton-pumping pyrophosphatase. *Biochem. J.* **337,** 373–377.
14. Cerius^2 Modeling Environment (1999) Molecular Simulations Inc., 4.0, San Diego.
15. Gasteiger, and Marsili, M. (1980) Iterative partial equalization of orbital electronegativity: a rapid access to atomic charges. *Tetrahedron* **36,** 3219–3222.
16. Hasegawa, K., and Funatsu, K. (2000) Partial least squares modeling and genetic algorithm optimization in quantitative structure-activity relationships. *SAR QSAR Environ. Res.* **11,** 189–209.
17. Szabo, C. M., Martin, M. B., and Oldfield, E. (2001) A quantitative 3D-QSAR/CoMFA investigation of *Dictyostelium discoideum* and bone growth inhibition by bisphosphonates. *J. Med. Chem.,* submitted.
18. Martin, M. B., Kendrick, H., Yardley, V., Lewis, J. C., Grimley, J. S., van Brussel, E. M., Olsen, J. R., Croft, S. L., and Oldfield, E. (2001) A 3D-QSAR/CoMFA study of the activity of bisphosphonates against *Trypanosoma brucei rhodesiense:* Farnesyl pyrophosphate synthase as a drug-target and an analysis of drug toxicity. *J. Med. Chem.,* submitted.
19. Szabo, C. M., Matsumura, Y., Fukura, S., Sengupta, S., Cieslak, J. A., Loftus, T. C., Lea, C. R., Martin, M. B., Lee, H.-J., Coates, R. M., Sagami, H., and Oldfield, E. (2001) A 3D-QSAR/CoMFA investigation of geranylgeranyl pyrophosphate synthase inhibition by bisphosphonates: A potential route to new bone resorption and anti-parasitic agents. *J. Med. Chem.,* submitted.
20. Martin, M. B., Arnold, W., III, H. T. H., Urbina, J. A., and Oldfield, E. (1999) Nitrogen-containing bisphosphonates as carbocation transition state analogues for isoprenoid biosynthesis. *Biochem. Biophys. Res. Commun.* **263,** 754–758.